Eulerian model of immersed elastic surfaces with full membrane elasticity

Thomas Milcent, Emmanuel Maitre

EULERIAN MODEL OF IMMERSED ELASTIC SURFACES WITH FULL MEMBRANE ELASTICITY. *

THOMAS MILCENT † AND EMMANUEL MAITRE ‡

Abstract. We introduce an Eulerian model for the coupling of a fluid governed by the Navier-Stokes equations, with an immersed interface endowed with full membrane elasticity (i.e. including shear effects). We show numerical evidences of its ability to account for large displacements/shear in a relatively simple way, avoiding some drawbacks of Lagrangian representation.

Key words. level set, fluid-structure, eulerian, immersed interface, Navier-Stokes, membrane elasticity

subject classifications. 74F10, 76D05, 65M06

1. Introduction In biomechanics of immersed membranes, the ability for a numerical model and method to handle shear efficiently is a challenging issue. Human red blood cells (RBCs) are among the simplest animal cells, since they have no nucleus nor organelle. They are made, like vesicles, of a phospholipid bilayer, plus a protein network (of spectrin), the cytoskeleton. For simple vesicles, the involved energy is a curvature energy, which is minimized with an area and enclosed volume constraint. In that case, Eulerian and Lagrangian models were developed in the last decade and proved to successfully reproduce the dynamics of such objects in flow [5, 8, 7, 9, 6, 11]. For the red blood cells the cytoskeleton provides an extra resistance to membrane shear. Capsules are usually constituted of a liquid drop protected by a thin elastic membrane. They are used for applications in cosmetic, food, and pharmaceutical industries. They are more rigid objects than vesicles, so that the curvature energy is small compared to membrane elasticity, including shear. In the modeling of vesicles or capsules, taking into account shear efficiently is of paramount interest.

On one hand, the definition of local shear variation on a surface is apparently easy in Lagrangian coordinates, and in the context of capsules, has been formalized decades ago [25, 2, 3]. However, when it comes to practical computations, the unavoidable singularity of Lagrangian parametrization of closed surfaces brings high complications [28, 27]. Moreover, large deformation and volume conservation in this Lagrangian setting also rise numerous difficulties, which were studied by several authors in the framework of the immersed boundary method [21, 17]. On the other hand, interface capturing methods using level-set, while more intrinsic and dimension-independent regarding surface localization, are usually reported as unable to capture tangential motions (see however somehow connected studies on surface flows and multicomponent vesicles [29, 18, 12]). This is due to the fact that the transport equation for the level-set function, namely $\partial_t\phi + u\cdot\nabla\phi = 0$, while recording some information on the surface area variations (enabling a complex fluid formulation of fluid-interface coupling [8, 9, 4]) just ignore any tangential component of u, since $\nabla\phi$ is normal to the interface.

However, full 3D Eulerian elasticity and its coupling with fluid mechanics has already successfully been studied and implemented numerically by several teams both

*Received date / Revised version date

†Institut de Mécanique de Bordeaux (I2M), Université de Bordeaux and Arts et Métiers ParisTech, France (thomas.milcent@u-bordeaux.fr).

‡Laboratoire Jean Kuntzmann, Université de Grenoble-Alpes and CNRS, France (emmanuel.maitre@imag.fr).

in the incompressible [10, 19, 30, 23, 24, 26] and compressible [15, 13] cases. The method relies on backward characteristics (also called reference map by some authors) which map back material points to their initial positions. This concept was also introduced early for point correspondence in level-set applied to image processing [22] and more recently to improve numerical accuracy of advection equations (e.g. level-set motions) [16, 20].

This article is a first attempt, to the best of our knowledge, to write a full Eulerian model of an immersed interface endowed with full membrane elasticity (i.e. including shear effects) and to provide numerical evidences of its ability to account for large displacements/shear in a relatively simple way.

In section 2, we recall the basic definitions of interface capturing via level-set and backward characteristics. In section 3 we provide simple examples illustrating the possible drawbacks of a Lagrangian approach to record shear variations. In section 4, we build two invariants that will be used to record the full membrane elasticity. The first one records area change (in both compressible and incompressible settings), while the second measures shear. In section 5, we consider the fluid-structure coupling problem: an immersed membrane into an incompressible fluid. The whole model is reduced, following [10] to a Navier-Stokes equation with source terms expressed as a combination of partial derivatives of the backward characteristics, coupled with the vectorial transport equation giving these characteristics. We provide numerical illustrations of the ability of the numerical implementation of our model to simulate the dynamic relaxation of an initially sheared sphere. As the notion of shear is best understood through simple tests, we provide in the Annex A analytical examples of velocity fields under which the deformed continuous medium actually experiences a shear, and show that our invariants behave as expected. The Annex B deals with some technical lemmas.

2. Preliminaries

2.1. Forward and backward characteristics Let $\Omega_0 \subset \mathbb{R}^3$ be the reference configuration of a continuous medium and assume that this medium is deformed by a smooth map $X : \mathbb{R}^3 \times \mathbb{R}^+ \longrightarrow \mathbb{R}^3$ (the forward characteristics) to $\Omega_t = X(\Omega_0, t)$. A velocity field $u : \mathbb{R}^3 \times \mathbb{R}^+ \longrightarrow \mathbb{R}^3$ is naturally associated with X:

$$\partial_t X(\xi,t) = u(X(\xi,t),t), \qquad X(\xi,0) = \xi, \qquad \xi \in \Omega_0. \tag{2.1}$$

We introduce the backward characteristics $Y : \mathbb{R}^3 \times \mathbb{R}^+ \longrightarrow \mathbb{R}^3$ by the formula $Y(X(\xi,t),t) = \xi$ (see Fig 2.1). The physical interpretation of $Y(x,t)$ is the position at time 0 of a material particle lying in x at time t and moving at speed u. The derivative of this relation with respect to t and ξ in turn gives with (2.1)

$$\partial_t Y + (u \cdot \nabla_x) Y = 0 \qquad\qquad Y(x,0) = x, \qquad x \in \Omega_t, \tag{2.2}$$

and

$$[\nabla_\xi X(\xi,t)] = [\nabla_x Y(x,t)]^{-1} \quad \text{for } x = X(\xi,t). \tag{2.3}$$

In the following, we use the notation ∇_ξ for the gradient with respect to ξ and we denote by ∇ the gradient with respect to x.

2.2. Eulerian representation of surfaces We consider a surface Γ_t captured by a level set function $\phi : \mathbb{R}^3 \times \mathbb{R}^+ \longrightarrow \mathbb{R}$

$$\Gamma_t = \{x \in \mathbb{R}^3 \,/\, \phi(x,t) = 0\}.$$

The initial position of the interface Γ_0 is associated to a given function ϕ_0 (thus we set $\phi(\cdot,0)=\phi_0$). We assume that the interface is advected by the velocity field u, so that ϕ verifies:

$$\partial_t\phi + u\cdot\nabla\phi = 0. \tag{2.4}$$

We have with (2.2) that the solution of (2.4) is given by

$$\phi(x,t) = \phi_0(Y(x,t)). \tag{2.5}$$

Let the normal in the reference configuration be denoted by $n_0(\xi)$ for $\xi\in\Gamma_0$, and the normal in the deformed configuration by $n(x,t)$ for $x\in\Gamma_t$ (See Fig 2.1). These normals are expressed in terms of normalized gradient of the associated level set:

$$n(x,t) = \frac{\nabla\phi(x,t)}{|\nabla\phi(x,t)|}, \qquad n_0(\xi) = \frac{\nabla_\xi\phi_0(\xi)}{|\nabla_\xi\phi_0(\xi)|}. \tag{2.6}$$

The relation (2.5) gives $\nabla\phi(x,t) = [\nabla Y(x,t)]^T\nabla\phi_0(Y(x,t))$, therefore with the definitions (2.6),

$$n_0(Y(x,t)) = \frac{[\nabla Y(x,t)]^{-T}n(x,t)}{|[\nabla Y(x,t)]^{-T}n(x,t)|}. \tag{2.7}$$

With (2.3), we get the Lagrangian equivalent of (2.7):

$$n(X(\xi,t),t) = \frac{[\nabla_\xi X(\xi,t)]^{-T}n_0(\xi)}{|[\nabla_\xi X(\xi,t)]^{-T}n_0(\xi)|}. \tag{2.8}$$

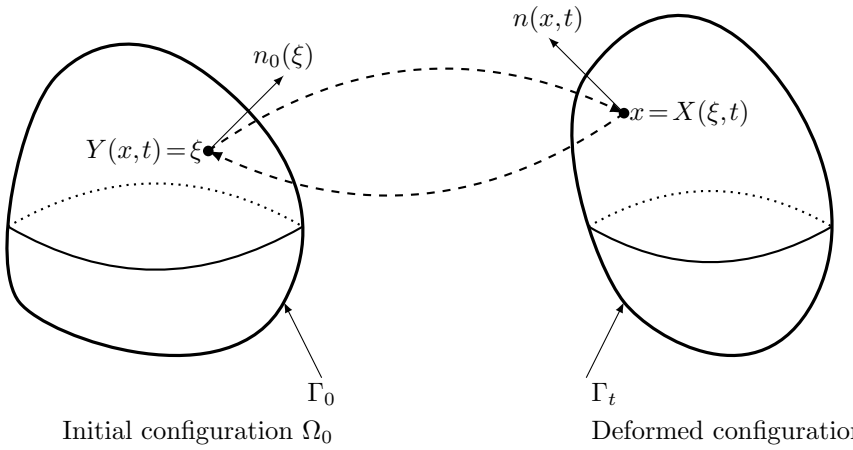

Fig. 2.1: Initial and deformed configurations

3. Can we measure surface shear variation with a Lagrangian description of the surface? We present in this section two intuitive methods to measure shear variation with a parametrization of the surface. The first one is based on the angle between two normalized vectors and the second one uses the invariants of the

metric tensor. We will show that even in the simplest case of a plane deformed in a shear velocity field, the two methods fail because the shear variation depends on the choice of initial parametrization. For general closed surfaces more difficulties arise from the singularity of Lagrangian parametrizations. The first method can not be applied because it is impossible to construct the normalized vectors (Hairy Ball theorem). We will show that for a sphere deformed in a shear velocity field the invariant of the second method is discontinuous at the poles. In any case the definition of shear depends completely on the choice of the parametrization and hence there is no canonical reference state. The limitations of these methods advocate for an immersion of the surface in $\mathbb{R}^3$ using a Eulerian description to capture shear.

3.1. Two Lagrangian methods to capture shear Let Γ_0 be the initial surface described by the parametrization $\Psi_0 : U \longrightarrow \mathbb{R}^3$ where U is an open subset of $\mathbb{R}^2$. A parametrization of the deformed surface Γ_t is given by $\Psi : U \times \mathbb{R}^+ \longrightarrow \mathbb{R}^3$ where $\Psi(\theta_1,\theta_2,t) = X(\Psi_0(\theta_1,\theta_2),t)$ and the deformed vectors associated to the parametrization are given by $a_i(t) = \partial_{\theta_i}\Psi(\theta_1,\theta_2,t)$. The first intuitive method to capture shear is to consider the angle between the two normalized deformed vectors

$$\text{angle}(t) = \arccos\left(\frac{a_1(t)}{|a_1(t)|}\cdot\frac{a_2(t)}{|a_2(t)|}\right).$$

The second one is to consider the metric tensor

$$\mathcal{M}(t) := \begin{pmatrix} a_1(t)\cdot a_1(t) & a_1(t)\cdot a_2(t) \\ a_1(t)\cdot a_2(t) & a_2(t)\cdot a_2(t) \end{pmatrix}$$

which is classically used to compute area, angles, and length of curves on the surface. The trace of $\mathcal{M}(t)$ captures shear deformation but contains also information on local area. Dividing the trace by the square root of the determinant keeps only shear effects, as will be illustrated below. We thus introduce the following invariants

$$\mathcal{Z}_1(t) = \sqrt{\det(\mathcal{M}(t))}, \qquad \mathcal{Z}_2(t) = \frac{\text{Tr}(\mathcal{M}(t))}{2\sqrt{\det(\mathcal{M}(t))}}, \tag{3.1}$$

where $\mathcal{Z}_1(t)$ correspond to the local area, and we will show that $\mathcal{Z}_2(t)$ is a good Lagrangian candidate to capture the local shear. In the following we are interested in the local variation of area and shear between time 0 and t. Therefore we consider the quantity $\text{angle}(t)/\text{angle}(0)$ and the invariants $\mathcal{Z}_i(t)/\mathcal{Z}_i(0)$. On the following examples we consider the shear velocity field (see Fig 7.10) with the associated forward characteristics given by:

$$u(x,y,z,t) = \begin{pmatrix} 0 \\ x \\ 0 \end{pmatrix}, \qquad X(\xi_1,\xi_2,\xi_3,t) = \begin{pmatrix} \xi_1 \\ \xi_2 + t\xi_1 \\ \xi_3 \end{pmatrix}.$$

3.2. Case of the plane: orthogonal parametrization Let Γ_0 be the plane $\{(x,y,z) \in \mathbb{R}^3 / z = 0\}$ which is parametrized by $\Psi_0 : \mathbb{R}^2 \longrightarrow \mathbb{R}^3$ given by:

$$\Psi_0 : (\theta_1,\theta_2) \mapsto \begin{pmatrix} \cos(\alpha)\theta_1 - \sin(\alpha)\theta_2 \\ \sin(\alpha)\theta_1 + \cos(\alpha)\theta_2 \\ 0 \end{pmatrix}.$$

where $\alpha \in [0,2\pi]$ is a parameter. The deformed surface Γ_t is still geometrically Γ_0 in this case and the deformed vectors are given by

$$a_1(t) = \begin{pmatrix} \cos(\alpha) \\ \sin(\alpha) + t\cos(\alpha) \\ 0 \end{pmatrix}, \qquad a_2(t) = \begin{pmatrix} -\sin(\alpha) \\ \cos(\alpha) - t\sin(\alpha) \\ 0 \end{pmatrix}.$$

At $t=0$ these vectors are orthonormal and have an α angle with the canonical basis (see Fig 3.1). We can show that for this example we have

$$\frac{\text{angle}(t)}{\text{angle}(0)} = \frac{2}{\pi}\arccos\left(\frac{t(2\cos(2\alpha) - t\sin(2\alpha))}{2\sqrt{(1+t\sin(2\alpha)+t^2\cos(\alpha)^2)(1-t\sin(2\alpha)+t^2\sin(\alpha)^2)}}\right). \quad (3.2)$$

This quantity depends on the angle parameter α (even if all pair of initial vectors are orthonormal). Hence this first method is not appropriate to measure the local shear variation. For the second method, the invariants (3.1) in the case of the plane are given by

$$\frac{\mathcal{Z}_1(t)}{\mathcal{Z}_1(0)} = 1, \qquad \frac{\mathcal{Z}_2(t)}{\mathcal{Z}_2(0)} = 1 + \frac{t^2}{2}. \quad (3.3)$$

Hence there is no area variation, the shear is constant in space and increase in time which correspond intuitively to what we can expect of a shear deformation. The second invariant is independent of α so this second method seems appropriate to capture shear.

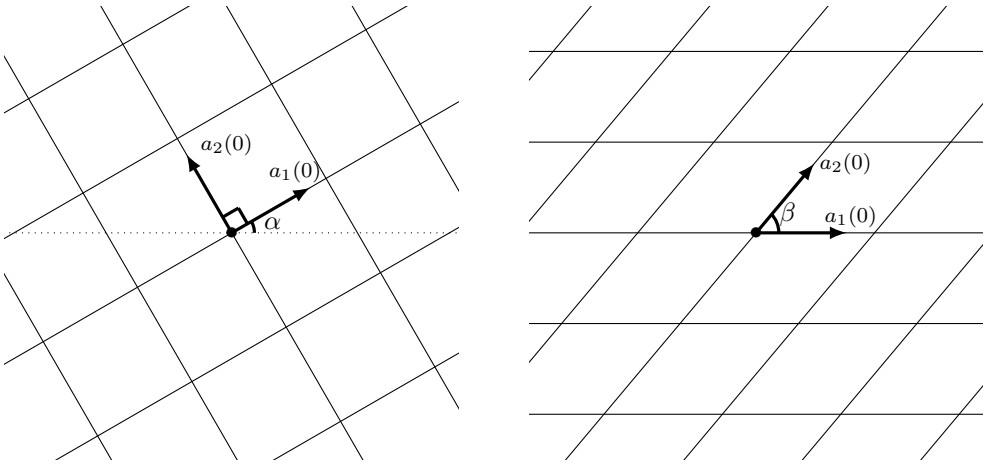

Fig. 3.1: Orthogonal (left) and non orthogonal (right) parametrization of the plane

3.3. Case of the plane: non orthogonal parametrization Let Γ_0 be the same plane $\{(x,y,z) \in \mathbb{R}^3 / z = 0\}$ described with another parametrization $\Psi_0 : \mathbb{R}^2 \longrightarrow \mathbb{R}^3$ given by:

$$\Psi_0 : (\theta_1, \theta_2) \mapsto \begin{pmatrix} \theta_1 + \cos(\beta)\theta_2 \\ \sin(\beta)\theta_2 \\ 0 \end{pmatrix}.$$

where $\beta \in [0,2\pi]$ is a parameter. The deformed vectors are given by

$$a_1(t) = \begin{pmatrix} 1 \\ t \\ 0 \end{pmatrix}, \qquad a_2(t) = \begin{pmatrix} \cos(\beta) \\ \sin(\beta) + t\cos(\beta) \\ 0 \end{pmatrix}.$$

At $t=0$ these vectors are not orthogonal and have an β angle (see Fig 3.1). For the second method, the invariants (3.1) are given by

$$\frac{\mathcal{Z}_1(t)}{\mathcal{Z}_1(0)} = 1, \qquad \frac{\mathcal{Z}_2(t)}{\mathcal{Z}_2(0)} = \frac{1}{2}\left(1 + t^2 + \cos(\beta)^2 + (t\cos(\beta) + \sin(\beta))^2\right) \tag{3.4}$$

There is no area variation and the shear depends on the parameter β. Therefore the second method fails to capture local shear variation because it depends on the choice of the parametrization.

3.4. Case of the sphere: orthogonal parametrization Let Γ_0 be the sphere $\{(x,y,z) \in \mathbb{R}^3 / x^2 + y^2 + z^2 = 1\}$ which is parametrized by $\Psi_0 : [0,\pi] \times [0,2\pi] \longrightarrow \mathbb{R}^3$ given by:

$$\Psi_0 : (\theta_1, \theta_2) \mapsto \begin{pmatrix} \sin(\theta_1)\cos(\theta_2) \\ \sin(\theta_1)\sin(\theta_2) \\ \cos(\theta_1) \end{pmatrix}.$$

The deformed vectors are given by

$$a_1(t) = \begin{pmatrix} \cos(\theta_1)\cos(\theta_2) \\ \cos(\theta_1)\sin(\theta_2) + \cos(\theta_1)\cos(\theta_2)t \\ -\sin(\theta_1) \end{pmatrix},$$
$$a_2(t) = \begin{pmatrix} -\sin(\theta_1)\sin(\theta_2) \\ \sin(\theta_1)\cos(\theta_2) - \sin(\theta_1)\sin(\theta_2)t \\ 0 \end{pmatrix}.$$

At $t=0$ these vectors are orthogonal (see Fig 3.2). The first method with angle between vectors will also failed in this more complex case. Indeed it is impossible to construct a continuous tangent vector field on a sphere (Hairy Ball theorem). For the second method, the invariants (3.1) in the case of the sphere are given by

$$\frac{\mathcal{Z}_1(t)}{\mathcal{Z}_1(0)} = \sqrt{1 - t\sin(\theta_1)^2\sin(2\theta_2) + t^2\sin(\theta_1)^2\sin(\theta_2)^2}, \tag{3.5}$$

$$\frac{\mathcal{Z}_2(t)}{\mathcal{Z}_2(0)} = \frac{1 + \sin(\theta_1)^2 + t\cos(2\theta_1)\sin(2\theta_2) + \frac{t^2}{2}(1 + \cos(2\theta_1)\cos(2\theta_2))}{(1+\sin(\theta_1)^2)\sqrt{1 - t\sin(\theta_1)^2\sin(2\theta_2) + t^2\sin(\theta_1)^2\sin(\theta_2)^2}}. \tag{3.6}$$

The first invariant (3.5) is well defined and represents the local area variation. The limit at the poles ($\theta_1 = 0$ or $\theta_1 = \pi$) of the second invariant (3.6) is $\cos(\theta_2)^2 + (\sin(\theta_2) + t\cos(\theta_2))^2$ and depends of θ_2. Therefore there is a discontinuity of the second invariant at the poles. We can reparametrize periodically the surface but the algorithms are more complex. Moreover the results will always depends on the choice of the parametrisation, even in zones where there is no singularity.

To tackle this problem we propose to immerse the surface in $\mathbb{R}^3$ and project on it the 3D deformations. In this case we use the flat metric of $\mathbb{R}^3$ instead of metric of

the surface and thus avoid the singularities of parametrizations. Also the immersion in $\mathbb{R}^3$ will allow to get a reference state which not depends of the parametrization. Furthermore we will introduce Z_i the Eulerian equivalent of the Lagrangian invariants $\mathcal{Z}_i$. We will show that Z_1 is the classical and well known local area variation. We will demonstrate with a variety of analytical illustrations in the Annex A that Z_2 is a "good candidate" to record the local shear variation.

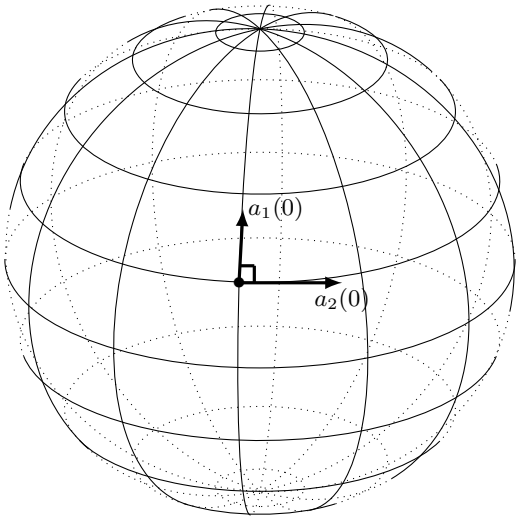

Fig. 3.2: Orthogonal parametrization of the sphere

4. Surface deformation in the Eulerian frame

4.1. The surface tensor $\mathcal{A}$ We want to measure the deformations on the surface Γ_t. Following the Lagrangian description of [25, 2, 3] we introduce the tensor

$$M(X(\xi,t),t) := [\nabla_\xi X(\xi,t)][\mathbb{I} - n_0(\xi)\otimes n_0(\xi)]. \tag{4.1}$$

Let $v(\xi)$ be a vector defined at the point $\xi \in \Gamma_0$. This vector is first projected with $[\mathbb{I} - n_0(\xi)\otimes n_0(\xi)]$ to $v_\tau(\xi) \in T_\xi\Gamma_0$, the tangent plane of Γ_0 at ξ. Then the vector $v_\tau(\xi)$ is deformed with X in the vector $[\nabla_\xi X(\xi,t)]v_\tau(\xi)$ at $X(\xi,t)$. A first property is that Mv is already in $T_{X(\xi,t)}\Gamma_t$, the tangent plane of Γ_t at $X(\xi,t)$. Indeed, using (2.8) and $v_\tau(\xi)\cdot n_0(\xi) = 0$, we have

$$(M(X(\xi,t),t)v(\xi))\cdot n(X(\xi,t),t) = ([\nabla_\xi X]^T n(X(\xi,t),t))\cdot v_\tau(\xi)) = 0$$

The tensor (4.1) is written in its Eulerian form with (2.3)

$$M(x,t) := [\nabla Y(x,t)]^{-1}[\mathbb{I} - n_0(Y(x,t))\otimes n_0(Y(x,t))].$$

The associate Cauchy-Green tensor is defined as ($\mathbb{I} - n_0\otimes n_0$ is a projector hence involutive)

$$\mathcal{A} := MM^T = [\nabla Y]^{-1}(\mathbb{I} - n_0(Y)\otimes n_0(Y))[\nabla Y]^{-T}.$$

After introducing the right Cauchy-Green tensor

$$B = [\nabla_\xi X][\nabla_\xi X]^T = [\nabla Y]^{-1}[\nabla Y]^{-T}, \tag{4.2}$$

using (2.7), the relation $A(v\otimes v)A^T = (Av)\otimes(Av)$ and $|[\nabla Y]^{-T}n|^2 = (Bn)\cdot n$ we get

$$\mathcal{A} = B - \frac{(Bn)\otimes(Bn)}{(Bn)\cdot n}. \tag{4.3}$$

4.2. Invariants of $\mathcal{A}$ According to (4.3) we have

$$\mathcal{A}n = 0. \tag{4.4}$$

Thus 0 is an eigenvalue and $\det(\mathcal{A}) = 0$. The other invariants are $\mathrm{Tr}(\mathcal{A})$ and $\mathrm{Tr}(\mathrm{Cof}(\mathcal{A})) = \frac{1}{2}(\mathrm{Tr}(\mathcal{A})^2 - \mathrm{Tr}(\mathcal{A}^2))$. As $\mathcal{A}$ is real and symmetric, there exists an orthonormal basis of eigenvectors. Moreover $\mathcal{A}$ is positive since $\mathcal{A}x\cdot x = |M^T x|^2 \geq 0$, so we denote its eigenvalues by 0, λ_1^2 and λ_2^2. Therefore $\mathrm{Tr}(\mathcal{A}) = \lambda_1^2 + \lambda_2^2$ and $\mathrm{Tr}(\mathrm{Cof}(\mathcal{A})) = (\lambda_1\lambda_2)^2$. We introduce the following invariants:

$$Z_1 = \sqrt{\mathrm{Tr}(\mathrm{Cof}(\mathcal{A}))} = |\lambda_1\lambda_2|, \tag{4.5}$$

$$Z_2 = \frac{\mathrm{Tr}(\mathcal{A})}{2\sqrt{\mathrm{Tr}(\mathrm{Cof}(\mathcal{A}))}} = \frac{1}{2}\left(\left|\frac{\lambda_1}{\lambda_2}\right| + \left|\frac{\lambda_2}{\lambda_1}\right|\right). \tag{4.6}$$

In the reference configuration (usually at initial time in our case), we have that $\mathcal{A}(0) = \mathbb{I} - n_0\otimes n_0$ so $\mathrm{Tr}(\mathcal{A}(0)) = 2$ and $\mathrm{Tr}(\mathrm{Cof}(\mathcal{A}(0))) = 1$. Under the smoothness assumption on u, there exists a time T that for $t < T$, $\mathrm{Tr}(\mathcal{A})$ and $\mathrm{Tr}(\mathrm{Cof}(\mathcal{A}))$ do not vanish. Therefore the invariant Z_2 is well defined. We have that $Z_1 = Z_2 = 1$ at initial time and the inequalities $Z_1 \geq 0$, $Z_2 \geq 1$. Note that Z_1 and Z_2 are both Eulerian fields, and we will derive in 5.2 equations to compute them. We will prove in the Annex B that Z_1 is exactly equal to the local area variation of the surface (even if incompressibility is not assumed on u). We will demonstrate in Annex A that Z_2 is a "good candidate" to record the local shear variation.

5. Immersed membrane in a fluid In this section we apply the above considerations to build an Eulerian fluid-structure model of an immersed elastic interface, which accounts for the full membrane elasticity through an energy involving invariants Z_1 and Z_2. We derive Eulerian equations verified by the two invariants, and the forces induced by the energy variation during the structure motion. The final model is recast as a Navier-Stokes system with a source term, the latter depending of space derivatives of Z_1 and Z_2, coupled with their Eulerian equations. This is a generalization to full membrane elasticity of a simple level-set formulation of the immersed boundary method that was introduced previously, and that we recall now.

5.1. Mathematical model We consider an elastic membrane Γ_t immersed into a fluid governed by e.g. incompressible Navier Stokes equations, lying in a bounded domain Ω of $\mathbb{R}^3$, for a time interval $[0,T]$. The interface Γ_t is captured by a level-set function $\phi : \Omega\times[0,T] \to \mathbb{R}$. Based on previous works on Eulerian description of immersed interface [8, 9] we write the coupling between the immersed surface and the surrounding fluid under the formulation:

$$\begin{cases} \partial_t u + u\cdot\nabla u - \frac{1}{R_e}\Delta u + \nabla p = f(\phi) & \text{on } \Omega\times[0,T] \\ \mathrm{div}\, u = 0 & \text{on } \Omega\times[0,T] \\ \partial_t\phi + u\cdot\nabla\phi = 0 & \text{on } \Omega\times[0,T] \end{cases}$$

where $f(\phi)$ accounts for the elastic force imparted on fluid by the immersed surface. Dependence on ϕ means here dependence on ϕ and its derivatives. We have shown that in the incompressible case, $|\nabla\phi|$ captures the local area variation and that the force associated to the regularized energy

$$\mathcal{E}=\int_\Omega E(|\nabla\phi|)\frac{1}{\varepsilon}\zeta\left(\frac{\phi}{\varepsilon}\right)\mathrm{d}x \tag{5.1}$$

can be expressed by the formula

$$f(\phi)=\mathrm{div}\left[E'(|\nabla\phi|)|\nabla\phi|\left(\mathbb{I}-\frac{\nabla\phi\otimes\nabla\phi}{|\nabla\phi|^2}\right)\frac{1}{\varepsilon}\zeta\left(\frac{\phi}{\varepsilon}\right)\right] \tag{5.2}$$

where $r\mapsto E(r)$ is the elastic constitutive law, ε the width of the interface and ζ is a cut-off function used to spread the interface near $\{\phi=0\}$. However in order to capture the full membrane energy, the function ϕ is not sufficient. Indeed a velocity field u tangential to Γ_t would verify $u\cdot\nabla\phi=0$ and therefore would not change the value of ϕ in its evolution equation. In order to capture some information on how points are moving on the surface, one way is to use the backward characteristics Y of the velocity field u. We propose the new model:

$$\begin{cases}\partial_t u+u\cdot\nabla u-\frac{1}{R_e}\Delta u+\nabla p=F_1(\phi,Y)+F_2(\phi,Y) & \text{on } \Omega\times[0,T]\\ \mathrm{div}\,u=0 & \text{on } \Omega\times[0,T]\\ \partial_t Y+u\cdot\nabla Y=0 & \text{on } \Omega\times[0,T]\end{cases} \tag{5.3}$$

where F_i is the force associated to the invariant Z_i, which expressions will be derived in the next section. In most cases, equations (5.3) will be supplemented with homogeneous initial and boundary conditions on the velocity, and with initial condition on Y given by identity:

$$u=0 \text{ on } \partial\Omega\times[0,T],\quad u=0 \text{ on } \Omega\times\{0\},\quad Y(0,x)=x \text{ on } \Omega.$$

Under such initial and boundary conditions, characteristics remain for all time inside Ω, thus the initial and deformed whole continuous medium (fluid and structure) always occupies the same domain of $\mathbb{R}^3$ (thus there is no need to introduce an initial and deformed configuration as in 2.1).

Moreover with such initial and boundary conditions, there is no need to solve an equation on ϕ, since the knowledge of Y and ϕ_0 is sufficient. Indeed the solution to the transport equation on ϕ is given by (see (2.5))

$$\phi(x,t)=\phi_0(Y(x,t)).$$

However if we consider an initially deformed interface (see (5.20) in the numerical tests), we could choose to set $Y(0,\cdot)$ to some maps not equal to identity. In that case, we need to solve the transport equation on ϕ

$$\partial_t\phi+u\cdot\nabla\phi=0. \tag{5.4}$$

Remark 5.1. *One could wonder about the optimality of our representation, regarding the number of fields to capture full membrane deformation. Note that to capture the interface position itself, we need one field (a level-set function ϕ). In the general*

case, to record the area change we need to compute Z_1 (or $|\nabla\phi|$ and J, see (8.1) in the Annex B), and therefore an extra field to get the shear. Thus as we solve for Y, which has three components, and obtain ϕ, Z_1 and Z_2 from it, we are optimal. In the incompressible case, area change is recorded by $|\nabla\phi|$ alone. We were not able, for the moment, to express shear by only introducing another field that we could compute without involving Y.

5.2. Eulerian equations on Z_i In order to build an Eulerian model we need to find evolution equations associated with Eulerian invariants.

PROPOSITION 5.1. *Under the smoothness assumption made on u, the invariants verify:*

$$\partial_t Z_1 + u\cdot\nabla Z_1 = Z_1\,[\nabla u]:\mathcal{C}_1, \qquad \mathcal{C}_1 = \mathbb{I} - n\otimes n, \tag{5.5}$$

$$\partial_t Z_2 + u\cdot\nabla Z_2 = Z_2\,[\nabla u]:\mathcal{C}_2, \qquad \mathcal{C}_2 = \frac{2\mathcal{A}}{\mathrm{Tr}(\mathcal{A})} - (\mathbb{I} - n\otimes n). \tag{5.6}$$

Proof. We first focus on the equations related to $\mathcal{A}$. Taking the gradient of (2.2), we get

$$\partial_t[\nabla Y] + u\cdot\nabla([\nabla Y]) = -[\nabla Y][\nabla u]$$

and its inverse verifies:

$$\partial_t([\nabla Y]^{-1}) + u\cdot\nabla([\nabla Y]^{-1}) = [\nabla u][\nabla Y]^{-1}. \tag{5.7}$$

The equation (4.2) on B is then given by

$$\partial_t B + u\cdot\nabla B = [\nabla u]B + B[\nabla u]^T. \tag{5.8}$$

Using (2.2) we get that

$$\partial_t(\mathbb{I} - n_0(Y)\otimes n_0(Y)) + u\cdot\nabla(\mathbb{I} - n_0(Y)\otimes n_0(Y)) = 0.$$

This relation together with (5.7) gives

$$\partial_t M + u\cdot\nabla M = [\nabla u]M, \qquad \partial_t M^T + u\cdot\nabla(M^T) = M^T[\nabla u]^T. \tag{5.9}$$

Using the relations (5.9) we get

$$\partial_t\mathcal{A} + u\cdot\nabla\mathcal{A} = [\nabla u]\mathcal{A} + \mathcal{A}[\nabla u]^T \tag{5.10}$$

where the initial condition is given by $\mathcal{A}(0) = \mathbb{I} - n_0\otimes n_0$. Note that B verifies the same equation (5.8) with a different initial condition $B(0) = \mathbb{I}$. Following (5.10), we get

$$\partial_t\,\mathrm{Tr}(\mathcal{A}) + u\cdot\nabla\,\mathrm{Tr}(\mathcal{A}) = 2[\nabla u]:\mathcal{A} \tag{5.11}$$

and

$$\partial_t\,\mathrm{Tr}(\mathrm{Cof}(\mathcal{A})) + u\cdot\nabla\,\mathrm{Tr}(\mathrm{Cof}(\mathcal{A})) = 2[\mathcal{A}\,\mathrm{Tr}(\mathcal{A}) - \mathcal{A}^2]:[\nabla u]. \tag{5.12}$$

Using (5.12) we get

$$\partial_t Z_1 + u\cdot\nabla Z_1 = Z_1\,\frac{[\mathcal{A}\,\mathrm{Tr}(\mathcal{A}) - \mathcal{A}^2]}{\mathrm{Tr}(\mathrm{Cof}(\mathcal{A}))}:[\nabla u].$$

We show in Lemma 8.1 of the Annex B that $\mathcal{A}\,\mathrm{Tr}(\mathcal{A}) - \mathcal{A}^2 = \mathrm{Tr}(\mathrm{Cof}(\mathcal{A}))[\mathbb{I} - n\otimes n]$. Using (5.11) and the equation on Z_1 we get the equation for Z_2. We have that $\mathcal{C}_i n = 0$ because $\mathcal{A}n = 0$ (see 4.4). We will prove in proposition 8.3 of Annex B that Z_1 captures the local area variation. In Annex A we provided a lot of illustrations to explain why Z_2 is a relevant measure of shear variation. □

5.3. Computation of the elastic forces F_i We introduce the regularized energy

$$\mathcal{E}_i = \int_\Omega E_i(Z_i)\frac{1}{\varepsilon}\zeta\left(\frac{\phi}{\varepsilon}\right)\mathrm{d}x. \tag{5.13}$$

Here E_i is the constitutive law associated to the invariant Z_i.

PROPOSITION 5.2. *The time variation of $\mathcal{E}_i$, using the principle of virtual power*

$$\partial_t \mathcal{E}_i = -\int_\Omega F_i \cdot u \,\mathrm{d}x \tag{5.14}$$

corresponds to the following force:

$$F_i = \nabla\left(E_i(Z_i)\frac{1}{\varepsilon}\zeta\left(\frac{\phi}{\varepsilon}\right)\right) + \mathrm{div}\left(E_i'(Z_i)Z_i\mathcal{C}_i\frac{1}{\varepsilon}\zeta\left(\frac{\phi}{\varepsilon}\right)\right). \tag{5.15}$$

Proof. The derivative with respect to t gives

$$\partial_t \mathcal{E}_i = \int_\Omega E_i'(Z_i)(Z_i)_t\frac{1}{\varepsilon}\zeta\left(\frac{\phi}{\varepsilon}\right)\mathrm{d}x + \int_\Omega E_i(Z_i)\frac{1}{\varepsilon^2}\zeta'\left(\frac{\phi}{\varepsilon}\right)\phi_t\,\mathrm{d}x.$$

Using the transport equation on ϕ and (5.5, 5.6) we get

$$\partial_t \mathcal{E}_i = \int_\Omega E_i'(Z_i)(-u\cdot\nabla Z_i + [\nabla u] : Z_i\mathcal{C}_i)\frac{1}{\varepsilon}\zeta\left(\frac{\phi}{\varepsilon}\right)\mathrm{d}x + \int_\Omega E_i(Z_i)\frac{1}{\varepsilon^2}\zeta'\left(\frac{\phi}{\varepsilon}\right)(-u\cdot\nabla\phi)\,\mathrm{d}x.$$

Integrating the second term by parts gives (the integral on $\partial\Omega$ vanishes since $\zeta(\frac{\phi}{\varepsilon}) = 0$ on $\partial\Omega$)

$$\partial_t \mathcal{E}_i = -\int_\Omega u\cdot\nabla(E_i(Z_i))\frac{1}{\varepsilon}\zeta\left(\frac{\phi}{\varepsilon}\right) + \mathrm{div}\left(E_i'(Z_i)Z_i\mathcal{C}_i\frac{1}{\varepsilon}\zeta\left(\frac{\phi}{\varepsilon}\right)\right)\cdot u + E_i(Z_i)u\cdot\nabla\left(\frac{1}{\varepsilon}\zeta\left(\frac{\phi}{\varepsilon}\right)\right)\mathrm{d}x.$$

Grouping the first and last term and using (5.14) leads to the expression (5.15). ∎

In the incompressible case, the gradient can be forgotten up to a redefinition of pressure and $Z_1 = |\nabla\phi|$ thanks to (8.1). Therefore we found the previous result (5.2). We have that

$$\mathrm{div}\left(E_i'(Z_i)Z_i\mathcal{C}_i\frac{1}{\varepsilon}\zeta\left(\frac{\phi}{\varepsilon}\right)\right) = \mathrm{div}\,(E_i'(Z_i)Z_i\mathcal{C}_i)\frac{1}{\varepsilon}\zeta\left(\frac{\phi}{\varepsilon}\right) + E_i'(Z_i)Z_i\mathcal{C}_i n\frac{|\nabla\phi|}{\varepsilon^2}\zeta'\left(\frac{\phi}{\varepsilon}\right).$$

The last term vanishes because $\mathcal{C}_i n = 0$. With the identity $\mathrm{div}(Av) = \mathrm{div}(A^T)\cdot v + A^T : \nabla v$ and the symmetry of $\mathcal{C}_i$ we get

$$\mathrm{div}\,(E_i'(Z_i)Z_i\mathcal{C}_i n) = 0 = \mathrm{div}\,(E_i'(Z_i)Z_i\mathcal{C}_i)\cdot n + E_i'(Z_i)Z_i\mathcal{C}_i : [\nabla n].$$

With the definition of $\mathcal{C}_1$ (5.5) and (5.6) we find the normal part of forces F_i (without the pressure term)

$$F_1\cdot n = -\,\mathrm{Tr}([\nabla n])E_1'(Z_1)Z_1\frac{1}{\varepsilon}\zeta\left(\frac{\phi}{\varepsilon}\right), \tag{5.16}$$

and with the relation $2Z_1Z_2=\mathrm{Tr}(\mathcal{A})$ (see (4.6)), we get

$$F_2\cdot n=-(2\mathrm{Tr}(\mathcal{A}[\nabla n])-\mathrm{Tr}(\mathcal{A})\mathrm{Tr}([\nabla n]))\frac{E_2'(Z_2)}{2Z_1}\frac{1}{\varepsilon}\zeta\left(\frac{\phi}{\varepsilon}\right). \tag{5.17}$$

In the previous formulas we used the relation $[\mathbb{I}-n\otimes n]:[\nabla n]=\mathrm{Tr}([\nabla n])$ ($[\nabla n]^T n=0$ since $|n|^2=1$) which is by definition the surface mean curvature. Hence the normal force associated to the area variation (5.16) only depends on the geometry through the surface curvature. The normal force associated to the shear variation (5.17) not only depends of the geometry but also of the deformations on the surface through $\mathcal{A}$. In the general case, the normal part of the shear force does not vanish.

5.4. Numerical method

The fluid-structure equations (5.3) and (5.4) are discretized with finite difference schemes on a staggered grid (see Fig 5.1 for a 2D configuration) with the classical projection method.

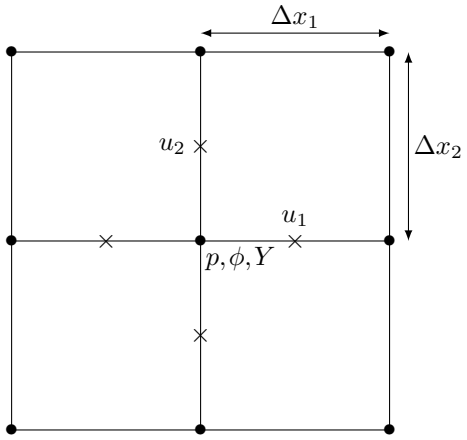

Fig. 5.1: Staggered grid with position of unknowns

Let Δt be the time step and u^n,p^n,ϕ^n,Y^n the time discretization of the variables at $t_n=n\Delta t$. The semi-discretization in time is given by

$$\text{Step 1:}\quad \frac{u^\star-u^n}{\Delta t}+u^n\cdot\nabla u^n-\frac{1}{R_e}\Delta u^n=F_1(\phi^n,Y^n)+F_2(\phi^n,Y^n)$$

$$\text{Step 2:}\quad \Delta p^{n+1}=\frac{\mathrm{div}(u^\star)}{\Delta t}$$

$$\text{Step 3:}\quad u^{n+1}=u^\star-\Delta t\nabla p^{n+1}$$

$$\text{Step 4:}\quad \frac{\phi^{n+1}-\phi^n}{\Delta t}+u^{n+1}\cdot\nabla\phi^n=0 \qquad \frac{Y^{n+1}-Y^n}{\Delta t}+u^{n+1}\cdot\nabla Y^n=0$$

In step 1 a prediction of the velocity is computed with an explicit Euler scheme in time and classical central staggered velocity-pressure schemes of order two for the convection, diffusion and the source terms. An explicit scheme in time is used for the diffusion because the Reynolds number is large enough. In step 2, the Poisson equation for the pressure is performed with the Fishpack library [1] (we use homogeneous

Neumann boundary conditions). In step 3 the the velocity is corrected to enforce the incompressibility condition. In step 4 the transport equations are discretiezd with an explicit Euler scheme in time and a WENO5 scheme in space [14].

We do not perform the redistancing. Instead, we use the renormalization $\frac{\phi}{|\nabla\phi|}$ to measure the distance to interface. Thus, $|\nabla\phi|\frac{1}{\varepsilon}\zeta\left(\frac{\phi}{\varepsilon}\right)$ is replaced by $\frac{1}{\varepsilon}\zeta\left(\frac{\phi}{|\nabla\phi|\varepsilon}\right)$. This approach was proved in [9] to be efficient from the point of view of both volume conservation and interface force calculations. For the cut-off function, we considered the following expression $\zeta(r)=\frac{1}{2}(1+\cos(\pi r))$ on $[-1,1]$ and $\zeta(r)=0$ elsewhere. We use in our simulations the linear elastic laws

$$E_1'(r)=\lambda(r-1) \qquad\qquad E_2'(r)=\mu(r-1) \tag{5.18}$$

where λ and μ are the elastic stretching and shear modulus (however the model is still strongly nonlinear due to the geometric nonlinearities and the coupling with Navier-Stokes equations).

5.5. Numerical tests In this section we provide evidences of numerical convergence of our method on the illustrative test case of a sheared elastic sphere. The domain $Q=[-1,1]^3$ is discretized on a Cartesian mesh with 128 points in each direction. We choose in our simulation a Reynolds number $R_e=100$, an elastic stretching modulus $\lambda=1$ and a shear modulus $\mu=0.1$. The parameter ε is equal to $3.5\Delta x$ in the simulations where Δx is the grid size. We take the time step $\Delta t=1.310^{-3}s$. We impose zero velocity for the initial and boundary conditions. The immersed initial surface is a sphere, so that

$$\phi_0(x,y,z)=\sqrt{x^2+y^2+z^2}-0.5, \tag{5.19}$$

but which is not in its rest state, since material points have been moved so that

$$Y(x,y,z,0)=(x\cos(t_0z)+y\sin(t_0z),-x\sin(t_0z)+y\cos(t_0z),z) \tag{5.20}$$

This corresponds to a deformation of the sphere when a 3D circular shear (see expression of Y for TC4 in Table 7.1 and Fig 7.8) is applied on opposite directions on the north and south poles (with respect to the z axis) until $t=t_0$. Here we take $t_0=\pi$. While this initial deformation was (artificially) imposed with no area variation (actually the sheared surface is still geometrically a sphere), the area will change when it starts to relax, so the force F_1 is also involved. The motion is however driven by F_2. The numerical results at different time steps are presented in Fig 5.2. For plotting purposes, we represented on the deformed surface a check board pattern which was tracked with markers, to visualize the shear relaxation. In Fig 5.3 we plot the velocity magnitude at $t=0.5s$, while the relaxation takes place. Due to the large imposed shear, the surface undergoes a complex deformation involving some small folds. These kind of ripples were also observed in [28] in the simulation of a capsule in a simple shear flow. A nice feature of our numerical code is its ability to relax toward a stable solution without any curvature energy. Some grid effects are however present for large time (see last picture of Fig 5.2). The use of an unstructured mesh and finite-element solver to remove this effect is presently under study.

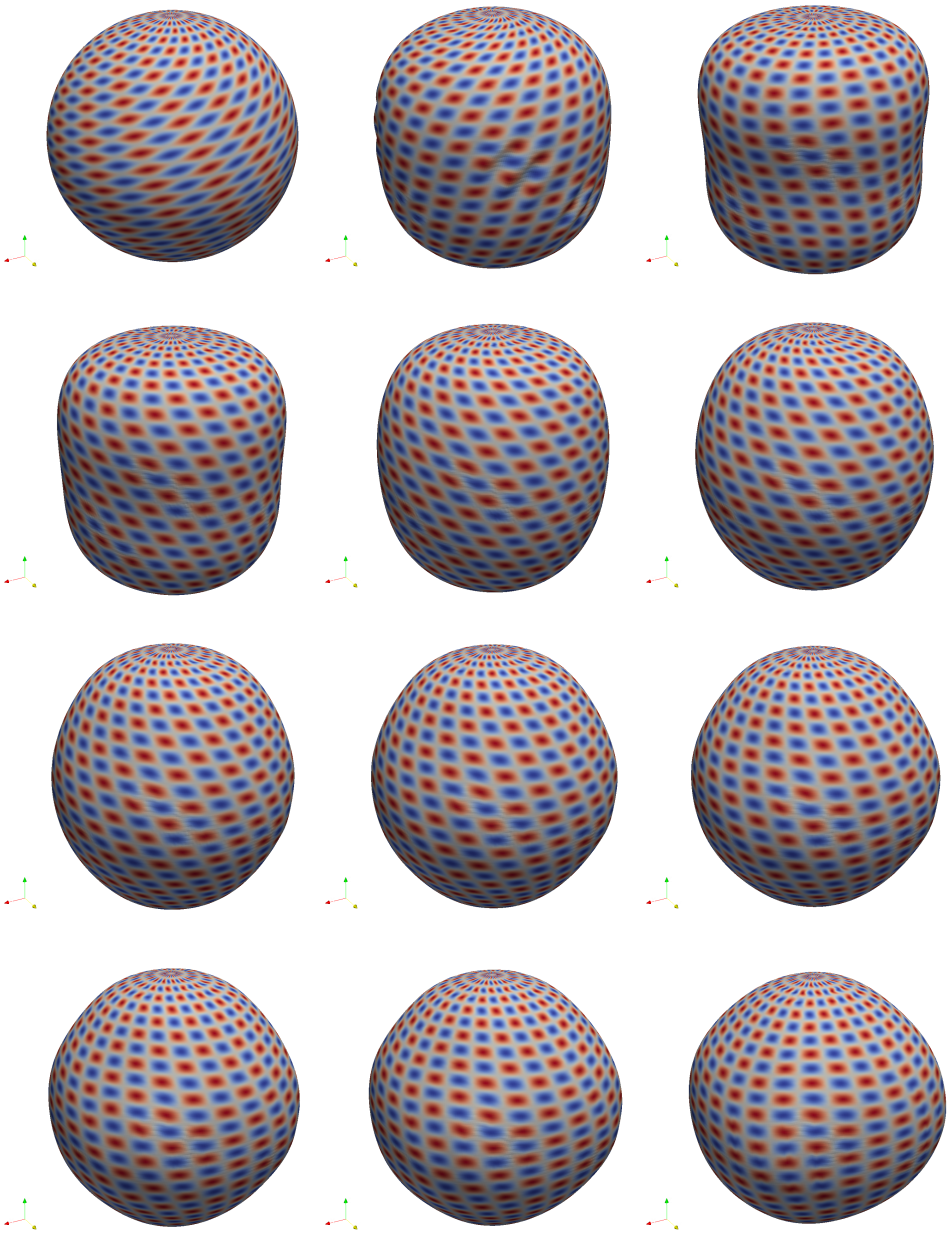

Fig. 5.2: Numerical simulation of the relaxation of a sphere due to shear force at times $t=0, 0.5s, 1s, 1.5s, 2s, 2.5s, 3s, 3.5, 4s, 4.5s, 5s, 9s$. Lagrangian markers are used for plotting a check board pattern coming back to undeformed state when shear decreases.

To provide more quantitative results, we plotted in Fig 5.4 and Fig 5.5 pressure slices following the x and z axis during this relaxation, for $t=0.1$ and $t=1.2$. The

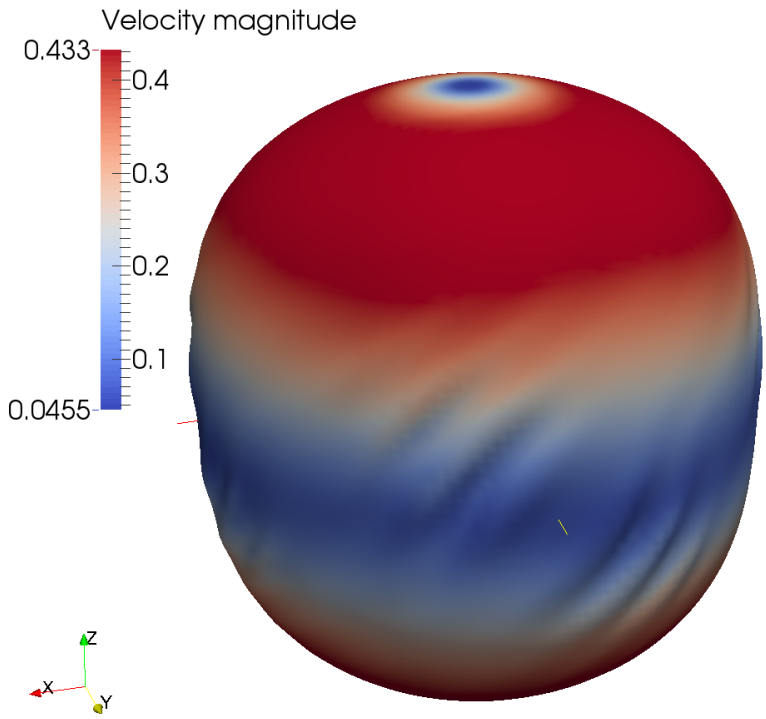

Fig. 5.3: Velocity magnitude at $t=0.5s$.

computation were performed with N points in each direction for three resolutions with $N=64,128,256$. Accordingly, we chose $\varepsilon=1.75\Delta x, 3.5\Delta x, 7\Delta x$ where Δx is the corresponding grid size, so that the numerical interface width remains constant. We observe numerical convergence. Likewise, Fig 5.6 depicts the variation of vertical radius during time.

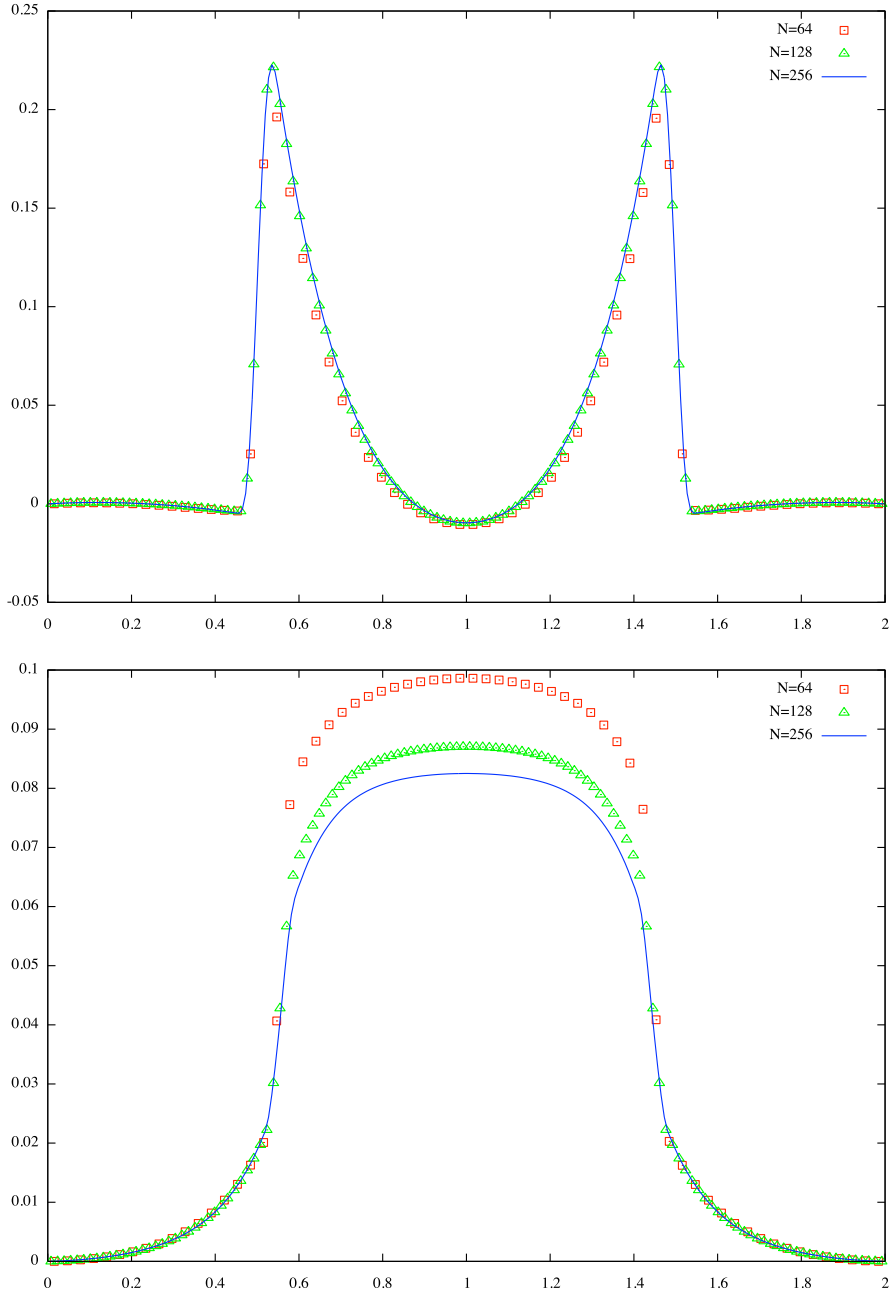

Fig. 5.4: Pressure along x axis at time $t=0.1$ (Top) and $t=1.2$ (Bottom) for $N=64,128,256$.

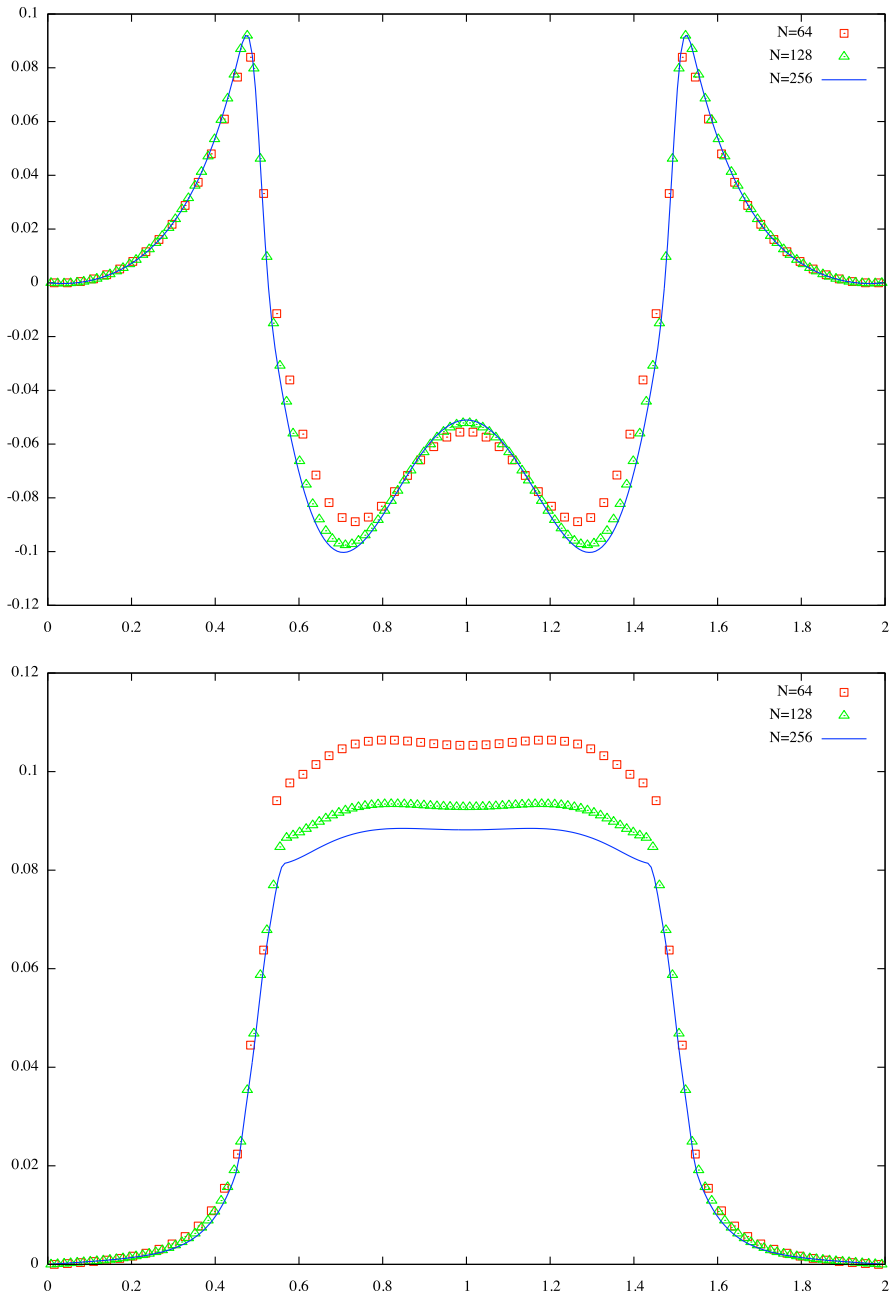

Fig. 5.5: Pressure along z axis at time $t=0.1$ (Top) and $t=1.2$ (Bottom) for $N=64,128,256$.

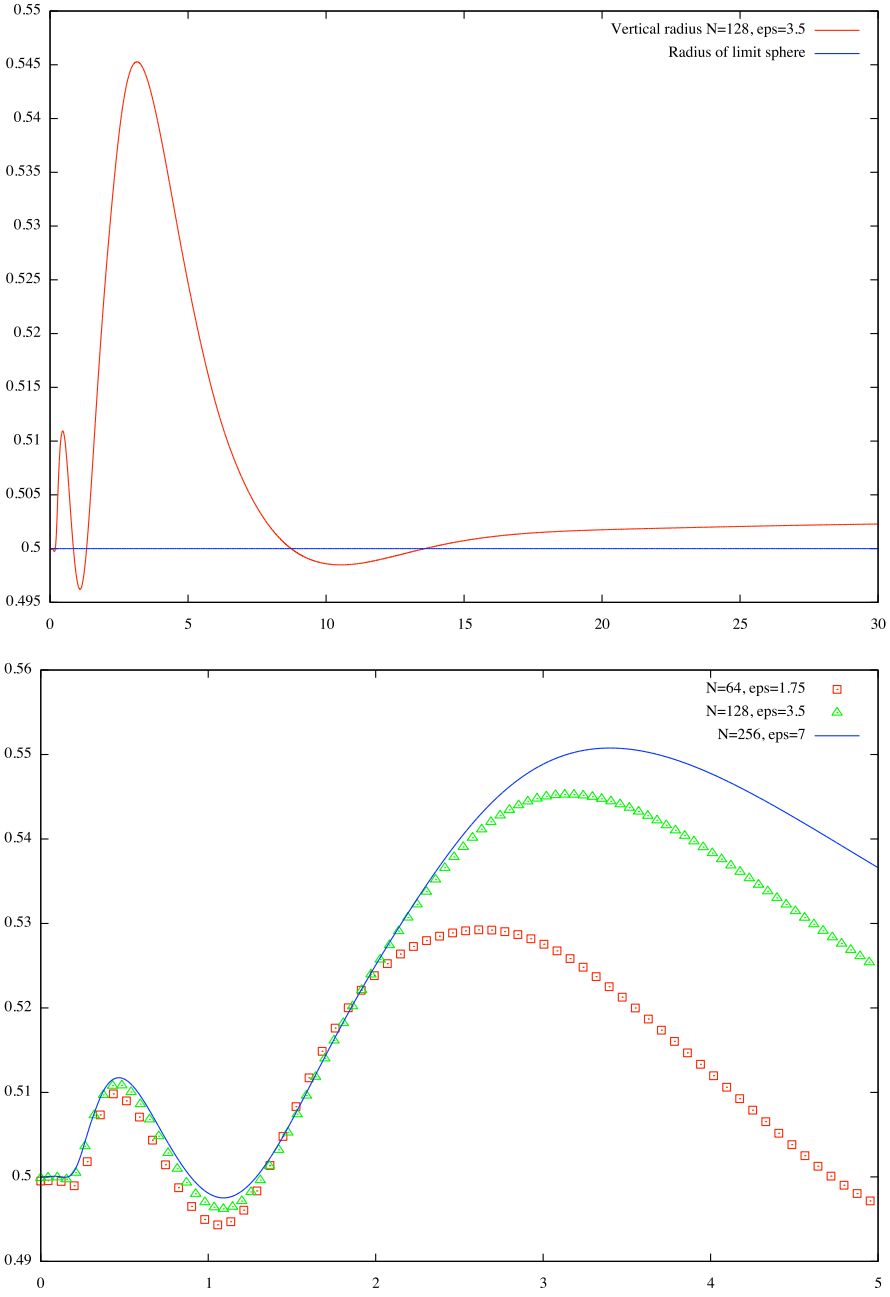

Fig. 5.6: Vertical radius up to $t=30$ (Top). Zoom on $t\in[0,5]$ for $N=64,128,256$.(Bottom)

As the flow is incompressible, the map $Y(\cdot,t):\Omega\to\Omega$ conserves volume, that is, $\det\nabla Y=1$ in the continuous case. However, after time and space discretization, and due to numerical errors introduce while solving for the transport equations on Y, such

nonlinear combination of derivatives will not fully respect this constraint. On Fig 5.7 and Fig 5.8, we depict the RMS (Root Mean Square) of $\det\nabla Y-1$ as a function of time, both for the whole domain, and on the interface. Thus the plotted quantities are respectively:

$$RMS_\Omega(t)=\left(\frac{1}{|\Omega|}\int_\Omega|\det\nabla Y(x,t)-1|^2\,\mathrm{d}x\right)^{\frac{1}{2}},$$
$$\text{and } RMS_{\Gamma_t}(t)=\left(\frac{1}{|\Gamma t|}\int_{\Gamma_t}|\det\nabla Y(x,t)-1|^2\,\mathrm{d}s\right)^{\frac{1}{2}}. \quad (5.21)$$

While $N=64$ is clearly under-resolved, the figures show numerical convergence of those RMS as N increases.

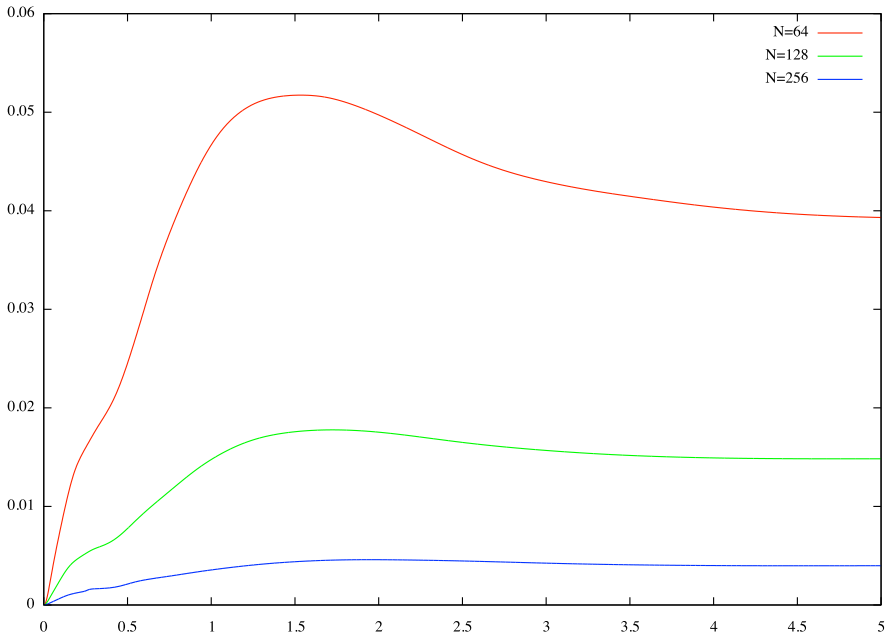

Fig. 5.7: Time evolution, for $N=64,128,256$ of $t\to RMS_\Omega(t)$ defined in (5.21).

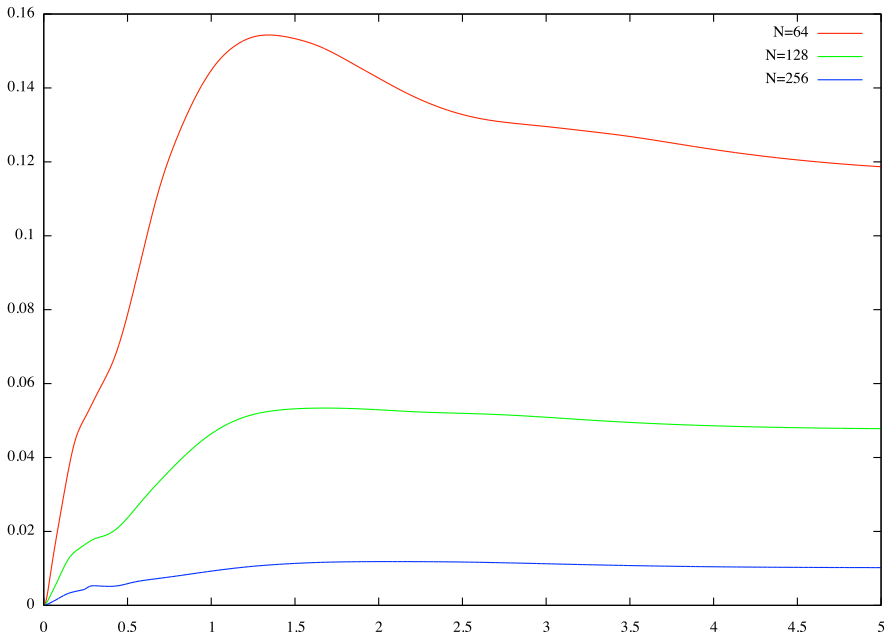

Fig. 5.8: Time evolution, for $N=64,128,256$ of $t\to RMS_{\Gamma_t}(t)$ defined in (5.21).

6. Conclusion In this paper we introduced a way to account for membrane shear in a completely Eulerian framework. The idea was to build two invariants from algebraic combinations of the space derivatives of the backward characteristics of the continuous medium velocity field. The first invariant accounts for changes of local area of the membrane, while the second records the local membrane shear. We showed how to compute those invariants in an Eulerian way, and produced some evidences that the second invariant indeed captures the membrane shear. The fluid-structure coupling is therefore rephrased as a Navier-Stokes equation with source term involving the two invariants, coupled to a vectorial transport equation for the backward characteristics. The formulation is therefore very versatile since it could be implemented as an add-on on a pre-existing fluid solver. In this first work, we presented outputs of a 3D numerical code using finite differences and a projection method on a staggered mesh, which simulate the relaxation of a spherical membrane which has been sheared from its poles. Our model and code is able to capture ripples due to the bucking of membrane, in a stable way without any extra smoothing curvature energy. Future work will focus on the application of this method to model red blood cells and capsules in 3D flows.

7. Annex A: Analytical illustrations for Z_2 We present some analytical illustrations to show that Z_2 is intuitively a "good" measure of the local shear variation of a surface. In all the test cases, we define an initial surface $\Gamma_0=\{\phi_0=0\}$ and a velocity field u which will move material points of this surface. Then we compute the backward characteristics Y and the invariants Z_1 and Z_2 to see how these Eulerian quantities could record this motion. The test cases and the results are described in Table 7.1.

7.1. Deformations where $\Gamma_t = \Gamma_0$ In this first serie of test cases (TC1 to TC4), while material points could have moved, globally the initial and deformed surface are the same ($\Gamma_0 = \Gamma_t$). Moreover, the deformations are uniform in space in the sense that the invariants Z_i on the surface do not depend on the spatial variables (except for TC4).

What we refer to the α and β deformations (TC1 and TC2) are $2D$ and the initial surface is the plane $z=0$. The velocity field of each deformation is plotted in the figures below with the corresponding values of Z_1 and Z_2. The $\beta=-1$ deformation is a rotation and as expected (slipping from hyperbolic to circular functions with $\sqrt{\beta}$ identified to $i \in \mathbb{C}$), there is no area variation and shear variation (see Fig 7.1). The $\alpha=1$ deformation is a pure dilatation and as expected, there is only area variation (see Fig 7.2). The $\beta=0$, $\beta=1$, $\alpha=-1$ deformations correspond to different shear transformations and as expected, there is only shear variation (see Fig 7.3, 7.4, 7.5). Note that for the $\beta=0$ test case we take the limit $\beta \longrightarrow 0$ the results for Y and Z_i. Moreover, for the $\beta=0$ deformation we found the same invariants as in the Lagrangian case (see (3.3)). The $\alpha=0$ deformation is an uniaxial deformation and there is area and shear variation (see Fig 7.6). It can be quite surprising at first sight, but when a surface is stretched in two directions with different magnitude ($\alpha \neq 1$) we do have shear and therefore as expected $Z_2 = \mathrm{ch}(t(1-\alpha)) \neq 1$. In the "3D circular shear" test cases the initial surfaces are a cylinder (TC3 see Fig 7.7) and a sphere (TC4 see Fig 7.8). In each plane $\{z=\alpha\}$ the velocity is a rotation of magnitude α. In these test cases there is no area variation, but pure shear variation. For TC3, $Z_2 = 1+\frac{t^2}{2}$ is constant on the surface ($x^2+y^2=1$ on the cylinder). This test case is clearly a 3D generalization on a cylinder of the 2D $\beta=0$ deformation and this is why we found the same invariants. For TC4, $Z_2 = 1+\frac{t^2}{2}(1-z^2)^2$ on the surface and depends only on the height z which is intuitive ($x^2+y^2+z^2=1$ on the sphere).

TC	$\phi_0(x,y,z)$	u	$Y(x,y,z,t)$	Z_1	Z_2
1	z	$\begin{pmatrix} x \\ \alpha y \\ 0 \end{pmatrix}$	$\begin{pmatrix} xe^{-t} \\ ye^{-\alpha t} \\ z \end{pmatrix}$	$e^{t(1+\alpha)}$	$\mathrm{ch}(t(1-\alpha))$
2	z	$\begin{pmatrix} \beta y \\ x \\ 0 \end{pmatrix}$	$\begin{pmatrix} x\mathrm{ch}(t\sqrt{\beta}) - y\sqrt{\beta}\mathrm{sh}(t\sqrt{\beta}) \\ -\frac{x}{\sqrt{\beta}}\mathrm{sh}(t\sqrt{\beta}) + y\mathrm{ch}(t\sqrt{\beta}) \\ z \end{pmatrix}$	1	$1+\frac{(1+\beta)^2}{2\beta}\mathrm{sh}^2(t\sqrt{\beta})$
3	x^2+y^2-1	$\begin{pmatrix} -yz \\ xz \\ 0 \end{pmatrix}$	$\begin{pmatrix} x\cos(tz)+y\sin(tz) \\ -x\sin(tz)+y\cos(tz) \\ z \end{pmatrix}$	1	$1+\frac{t^2}{2}(x^2+y^2)$
4	$x^2+y^2+z^2-1$	$\begin{pmatrix} -yz \\ xz \\ 0 \end{pmatrix}$	$\begin{pmatrix} x\cos(tz)+y\sin(tz) \\ -x\sin(tz)+y\cos(tz) \\ z \end{pmatrix}$	1	$1+\frac{t^2(x^2+y^2)^2}{2(x^2+y^2+z^2)}$
5	$x^2+y^2+z^2-1$	$\begin{pmatrix} x \\ y \\ z \end{pmatrix}$	$\begin{pmatrix} e^{-t}x \\ e^{-t}y \\ e^{-t}z \end{pmatrix}$	e^{2t}	1
6	$\max(\lvert x\rvert,\lvert y\rvert,\lvert z\rvert)-1$	$\begin{pmatrix} 0 \\ x \\ 0 \end{pmatrix}$	$\begin{pmatrix} x \\ y-tx \\ z \end{pmatrix}$	See (7.1)-(7.3)	
7	$x^2+y^2+z^2-1$	$\begin{pmatrix} 0 \\ x \\ 0 \end{pmatrix}$	$\begin{pmatrix} x \\ y-tx \\ z \end{pmatrix}$	See (7.4)	See (7.5)

Table 7.1: Table of test cases

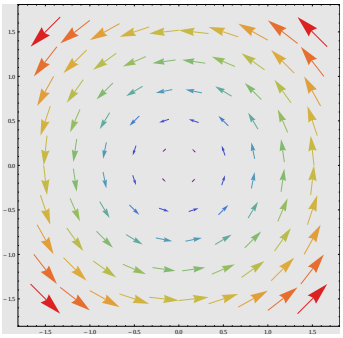

$Z_1 = 1 \qquad Z_2 = 1$

Fig. 7.1: Velocity field $(-y,x,0)$ of the $\beta = -1$ deformation (TC2)

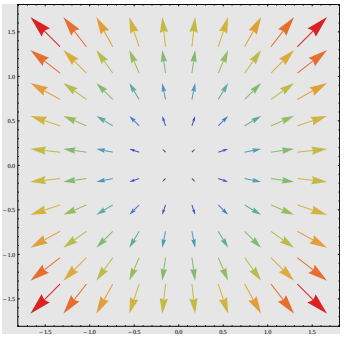

$Z_1 = e^{2t} \qquad Z_2 = 1$

Fig. 7.2: Velocity field $(x,y,0)$ of the $\alpha = 1$ deformation (TC1)

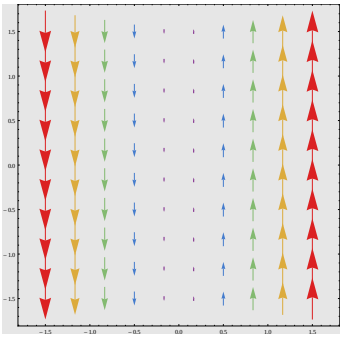

$Z_1 = 1 \qquad Z_2 = 1 + \frac{t^2}{2}$

Fig. 7.3: Velocity field $(0,x,0)$ of the $\beta = 0$ deformation (TC2)

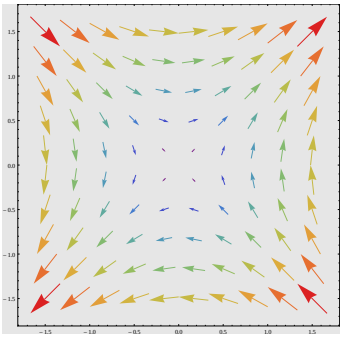

$Z_1 = 1 \qquad Z_2 = \mathrm{ch}(2t)$

Fig. 7.4: Velocity field $(y,x,0)$ of the $\beta = 1$ deformation (TC2)

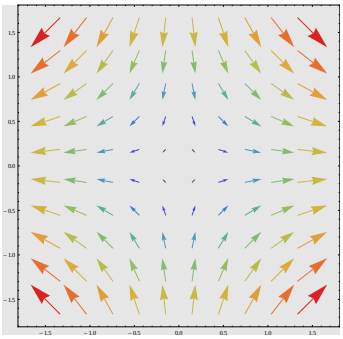

$Z_1 = 1 \qquad Z_2 = \mathrm{ch}(2t)$

Fig. 7.5: Velocity field $(x,-y,0)$ of the $\alpha = -1$ deformation (TC1)

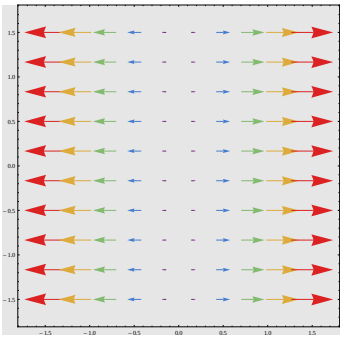

$Z_1 = e^t \qquad Z_2 = \mathrm{ch}(t)$

Fig. 7.6: Velocity field $(x,0,0)$ of the $\alpha = 0$ deformation (TC1)

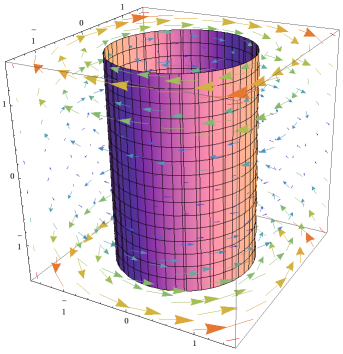

$Z_1 = 1 \qquad Z_2 = 1 + \frac{t^2}{2}(x^2+y^2)$

Fig. 7.7: Velocity field $(-yz, xz, 0)$ of the 3D circular shear and initial shape of the cylinder (TC3)

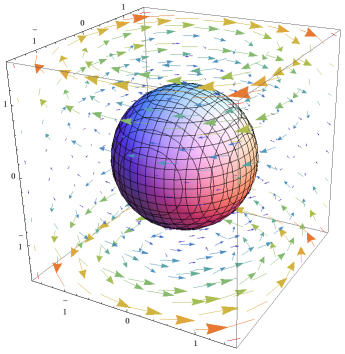

$Z_1 = 1 \qquad Z_2 = 1 + \frac{t^2(x^2+y^2)^2}{2(x^2+y^2+z^2)}$

Fig. 7.8: Velocity field $(-yz, xz, 0)$ of the 3D circular shear and initial shape of the sphere (TC4)

7.2. Deformations where $\Gamma_t \neq \Gamma_0$ We present now three test cases (TC5-7) where the deformed surface Γ_t is different of the initial shape Γ_0. For the 3D dilatation deformation (TC5 see Fig 7.9), the initial surface is a sphere. In this test case we have only area variation, as expected.

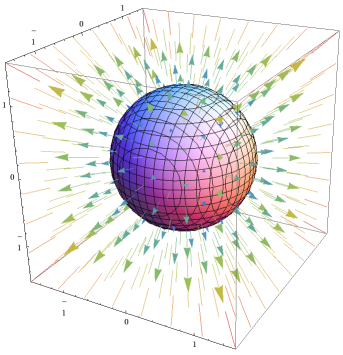

$Z_1 = e^{2t} \qquad Z_2 = 1$

Fig. 7.9: Velocity field (x, y, z) of the 3D dilatation and initial shape of the sphere (TC5)

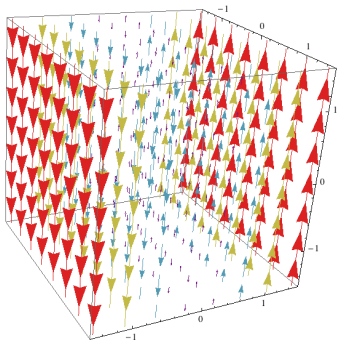

Fig. 7.10: Velocity field $(0, x, 0)$ of the shear deformation(TC6-7)

In the last test cases, the same shear velocity field (see Fig 7.10) is applied on a cube and on a sphere. For the test case TC6 the deformed shape of the cube (see Fig 7.11) is given by the zero level set of

$$\phi(x, y, z, t) = \max(|x|, |y - tx|, |z|) - 1.$$

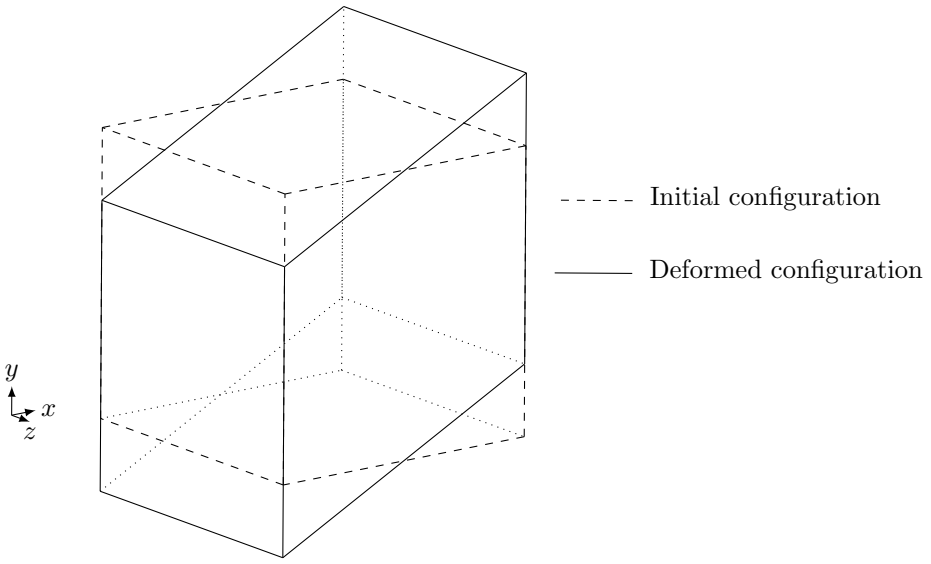

Fig. 7.11: Initial and deformed shape of the cube (TC6)

The calculations are done independently on each plane that composes the cube. We have the following results

$$\text{On the faces } \{x=\pm 1\} \qquad Z_1=1, \qquad Z_2=1 \tag{7.1}$$

$$\text{On the faces } \{y-tx=\pm 1\} \qquad Z_1=\sqrt{1+t^2} \qquad Z_2=\frac{2+t^2}{2\sqrt{1+t^2}} \tag{7.2}$$

$$\text{On the faces } \{z=\pm 1\} \qquad Z_1=1, \qquad Z_2=1+\frac{t^2}{2} \tag{7.3}$$

On the faces corresponding to $\{x=\pm 1\}$ there is no area and shear variation (the faces are just translated). For the faces of equations $\{y-tx=\pm 1\}$ the faces are stretched in only one direction and there is area and shear variation as in the 2D $\alpha=0$ deformation. For the faces $\{z=\pm 1\}$ there is only shear variation as in the 2D $\beta=0$ deformation.

For the test case TC7 the deformed shape of the sphere Γ_t is given by the zero level set of

$$\phi(x,y,z,t)=x^2+(y-tx)^2+z^2-1.$$

We have that

$$Z_1=\sqrt{1+t^2+\frac{t^2(x^2-z^2)-2txy}{x^2+(y-tx)^2+z^2}} \tag{7.4}$$

$$Z_2=\left(1+\frac{t^2}{2}+\frac{t^2x^2-2txy}{2(x^2+(y-tx)^2+z^2)}\right)\frac{1}{Z_1} \tag{7.5}$$

In Fig 7.12, iso-contours of Z_1 and Z_2 are plotted on the deformed surface Γ_t. The results are intuitive: the area variation reaches its maximum on points that are orthogonal to the $y=tx$ plane while the shear variation is larger along the z axis. The deformation and the initial surface are the same as in the Lagrangian test case in section

3.3. In the formula (7.5) there is no discontinuities at the poles $(x^2+(y-tx)^2+z^2=1$ on the surface $\Gamma_t)$ unlike in the Lagrangian formula (3.6)

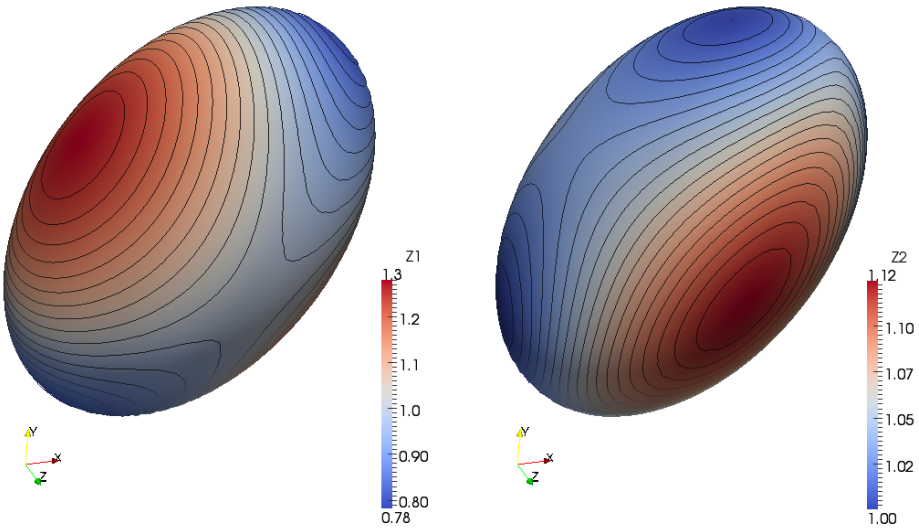

Fig. 7.12: Plot of iso-contours of Z_1 and Z_2 on the deformed surface at $t=0.5s$ (TC7)

8. Annex B

8.1. Technical lemma

LEMMA 8.1. *The following identity holds:*

$$\mathcal{A}\,\mathrm{Tr}(\mathcal{A})-\mathcal{A}^2=\mathrm{Tr}(\mathrm{Cof}(\mathcal{A}))[\mathbb{I}-n\otimes n].$$

Proof. It is equivalent to prove the lemma in any basis of $\mathbb{R}^3$. We consider the orthonormal basis of $\mathbb{R}^3$ $\mathcal{B}'=(e'_1,e'_2,e'_3)=(\tau_1,\tau_2,n)$ where (τ_1,τ_2) is an orthonormal basis of the tangent plane orthogonal to n. Let $\mathcal{A}'$ be the matrix of the tensor $\mathcal{A}$ in the basis $\mathcal{B}'$ and we denote by $\mathcal{A}'_{ij}$ its coefficients. We have with (4.4) that $\mathcal{A}n=0$, hence we have $\mathcal{A}'_{i3}=0$. Since $\mathcal{A}$ is a symmetric tensor and $\mathcal{B}'$ is an orthonormal basis, the matrix $\mathcal{A}'$ is a symmetric and its structure is given by:

$$\mathcal{A}'=\begin{pmatrix}\mathcal{A}'_{11} & \mathcal{A}'_{12} & 0\\ \mathcal{A}'_{12} & \mathcal{A}'_{22} & 0\\ 0 & 0 & 0\end{pmatrix}$$

and therefore

$$(\mathcal{A}')^2=\begin{pmatrix}(\mathcal{A}'_{11})^2+(\mathcal{A}'_{12})^2 & \mathcal{A}'_{11}\mathcal{A}'_{12}+\mathcal{A}'_{12}\mathcal{A}'_{22} & 0\\ \mathcal{A}'_{11}\mathcal{A}'_{12}+\mathcal{A}'_{12}\mathcal{A}'_{22} & (\mathcal{A}'_{12})^2+(\mathcal{A}'_{22})^2 & 0\\ 0 & 0 & 0\end{pmatrix}.$$

In the basis $\mathcal{B}'$ we have

$$\mathbb{I}-n\otimes n=\begin{pmatrix}1&0&0\\0&1&0\\0&0&0\end{pmatrix}$$

$\mathcal{A}'$ and $\mathcal{A}$ have the same invariants so

$$\begin{aligned}\mathrm{Tr}(\mathcal{A}) &= \mathrm{Tr}(\mathcal{A}') = \mathcal{A}'_{11} + \mathcal{A}'_{22}\\ \mathrm{Tr}(\mathrm{Cof}(\mathcal{A})) &= \mathrm{Tr}(\mathrm{Cof}(\mathcal{A}')) = \mathcal{A}'_{11}\mathcal{A}'_{22} - (\mathcal{A}'_{12})^2\end{aligned}$$

It is now easy to check that $\mathcal{A}'\mathrm{Tr}(\mathcal{A}') - (\mathcal{A}')^2 = \mathrm{Tr}(\mathrm{Cof}(\mathcal{A}'))[\mathbb{I} - n\otimes n]$ and the lemma is proved. □

8.2. Equivalent expression for Z_1 In this subsection we give an equivalent expression of Z_1 which links the present formulation with our previous work [9].

PROPOSITION 8.2. *Let $J = \det(\nabla_\xi X) = \det(\nabla Y)^{-1}$ be the volume ratio, then*

$$Z_1 = J\frac{|\nabla\phi|}{|\nabla\phi_0(Y)|}. \tag{8.1}$$

Proof. The invariant Z_1 is defined by (4.5)

$$Z_1 = \sqrt{\mathrm{Tr}(\mathrm{Cof}(\mathcal{A}))} \tag{8.2}$$

With the definition (4.3), we get

$$\mathrm{Tr}(\mathcal{A})^2 = \left(\mathrm{Tr}(B) - \frac{(B^2n)\cdot n}{(Bn)\cdot n}\right)^2$$

and

$$\mathrm{Tr}(\mathcal{A}^2) = \mathrm{Tr}(B^2) - 2\frac{(B^3n)\cdot n}{(Bn)\cdot n} + \left(\frac{(B^2n)\cdot n}{(Bn)\cdot n}\right)^2$$

Using the Cayley-Hamilton theorem $B^3 - \mathrm{Tr}(B)B^2 + \mathrm{Tr}(\mathrm{Cof}(B))B - \det(B)\mathbb{I} = 0$ we get

$$\mathrm{Tr}(\mathrm{Cof}(\mathcal{A})) = \frac{1}{(Bn)\cdot n}\left((B^3n)\cdot n - \mathrm{Tr}(B)(B^2n)\cdot n + \mathrm{Tr}(\mathrm{Cof}(B))(Bn)\cdot n\right) = \frac{\det(B)}{(Bn)\cdot n}$$

The gradient of (2.5) gives the relation $\nabla\phi = [\nabla Y]^T\nabla\phi_0(Y)$ so

$$(Bn)\cdot n = \left|[\nabla Y]^{-T}\frac{\nabla\phi}{|\nabla\phi|}\right|^2 = \frac{|\nabla\phi_0(Y)|^2}{|\nabla\phi|^2}$$

We have the relation $\det(B) = J^2$ so the expression of Z_1 (8.2) reduces to (8.1). This recovers the result of [9] where the area variation captured by $|\nabla\phi|$ in the incompressible case ($J = 1$). □

8.3. Proof that Z_1 is the local area variation

PROPOSITION 8.3. *Let Γ_0 a smooth surface, deformed with smooth forward characteristics in $\Gamma_t = X(\Gamma_0, t)$. We denote by u the associated smooth velocity field. Let a parametrization of the surface Γ_t be given by $(\theta_1,\theta_2)\mapsto\Psi(\theta_1,\theta_2,t)$ where $\Psi: U\times\mathbb{R}^+ \longrightarrow \mathbb{R}^3$ is smooth on an open set U of $\mathbb{R}^2$. The local area variation verifies*

$$\frac{|\Psi_{,1}(\theta_1,\theta_2,t)\wedge\Psi_{,2}(\theta_1,\theta_2,t)|}{|\Psi_{,1}(\theta_1,\theta_2,0)\wedge\Psi_{,2}(\theta_1,\theta_2,0)|} = \frac{Z_1(\Psi(\theta_1,\theta_2,t),t)}{Z_1(\Psi(\theta_1,\theta_2,0),0)} = \frac{Z_1(x,t)}{Z_1(Y(x,t),0)} \tag{8.3}$$

for $x=\Psi(\theta_1,\theta_2,t)$ *and with the notation* $\Psi_{,i}(\theta_1,\theta_2,t):=\partial_{\theta_i}\Psi(\theta_1,\theta_2,t)$.

Proof. Let $f:\mathbb{R}^3\times\mathbb{R}^+\longrightarrow\mathbb{R}$ be a smooth function. The Reynolds formula for surfaces reads

$$\frac{\mathrm{d}}{\mathrm{dt}}\left(\int_{\Gamma_t} f\,\mathrm{d}s\right)=\int_{\Gamma_t}\partial_t f+u\cdot\nabla f+f[\nabla u]:[\mathbb{I}-n\otimes n]\,\mathrm{d}s.$$

Let $g:\mathbb{R}^3\longrightarrow\mathbb{R}$ be smooth function and let $f(x,t)=\frac{g(Y(x,t))}{Z_1(x,t)}$. The expression in the previous integral becomes

$$\frac{1}{Z_1}\left(\partial_t(g(Y))+u\cdot\nabla(g(Y))\right)-\frac{g(Y)}{(Z_1)^2}\left(\partial_t Z_1+u\cdot\nabla Z_1-Z_1[\nabla u]:[\mathbb{I}-n\otimes n]\right)\qquad(8.4)$$

The first term vanishes with (2.2). The second term is also zero with (5.5). Therefore

$$\frac{\mathrm{d}}{\mathrm{dt}}\left(\int_{\Gamma_t}\frac{g(Y(x,t))}{Z_1(x,t)}\,\mathrm{d}s\right)=0\qquad(8.5)$$

Since $\Psi(\theta_1,\theta_2,0)=Y(\Psi(\theta_1,\theta_2,t),t)$ the equation (8.5) becomes

$$\int_U\frac{g(\Psi(\theta_1,\theta_2,0))}{Z_1(\Psi(\theta_1,\theta_2,t),t)}|\Psi_{,1}(\theta_1,\theta_2,t)\wedge\Psi_{,2}(\theta_1,\theta_2,t)|\,\mathrm{d}\theta_1\mathrm{d}\theta_2$$
$$=\int_U\frac{g(\Psi(\theta_1,\theta_2,0))}{Z_1(\Psi(\theta_1,\theta_2,0),0)}|\Psi_{,1}(\theta_1,\theta_2,0)\wedge\Psi_{,2}(\theta_1,\theta_2,0)|\,\mathrm{d}\theta_1\mathrm{d}\theta_2$$

This result holds for all function g. Therefore (8.3) holds and Z_1 measures the local area variation (in the compressible and incompressible cases). □

REFERENCES

[1] J.C. Adams, P.N. Swarztrauber, and R. Sweet. Fishpack - efficient fortran subprograms for the solution of separable elliptic partial differential equations. *http://www2.cisl.ucar.edu/resources/legacy/fishpack*.

[2] D Barthes-Biesel. Motion of a spherical microcapsule freely suspended in a linear shear flow. *Journal of Fluid Mechanics*, 100(04):831–853, 1980.

[3] D Barthes-Biesel and JM Rallison. The time-dependent deformation of a capsule freely suspended in a linear shear flow. *Journal of Fluid Mechanics*, 113:251–267, 1981.

[4] J Thomas Beale and John Strain. Locally corrected semi-lagrangian methods for stokes flow with moving elastic interfaces. *Journal of Computational Physics*, 227(8):3896–3920, 2008.

[5] J Beaucourt, F Rioual, T Séon, T Biben, and C Misbah. Steady to unsteady dynamics of a vesicle in a flow. *Physical Review E*, 69(1):011906, 2004.

[6] Thierry Biben, Alexander Farutin, and Chaouqi Misbah. Three-dimensional vesicles under shear flow: Numerical study of dynamics and phase diagram. *Physical Review E*, 83(3):031921, 2011.

[7] Thierry Biben, Klaus Kassner, and Chaouqi Misbah. Phase-field approach to three-dimensional vesicle dynamics. *Physical Review E*, 72(4):041921, 2005.

[8] Georges-Henri Cottet and Emmanuel Maitre. A level-set formulation of immersed boundary methods for fluid–structure interaction problems. *Comptes Rendus Mathematique*, 338(7):581–586, 2004.

[9] Georges-Henri Cottet and Emmanuel Maitre. A level set method for fluid-structure interactions with immersed surfaces. *Mathematical models and methods in applied sciences*, 16(03):415–438, 2006.

[10] Georges-Henri Cottet, Emmanuel Maitre, and Thomas Milcent. Eulerian formulation and level set models for incompressible fluid-structure interaction. *ESAIM: Mathematical Modelling and Numerical Analysis*, 42(03):471–492, 2008.

[11] Vincent Doyeux, Yann Guyot, Vincent Chabannes, Christophe Prudhomme, and Mourad Ismail. Simulation of two-fluid flows using a finite element/level set method. application to bubbles and vesicle dynamics. *Journal of Computational and Applied Mathematics*, 246:251–259, 2013.

[12] Knut Erik Teigen, Peng Song, John Lowengrub, and Axel Voigt. A diffuse-interface method for two-phase flows with soluble surfactants. *Journal of computational physics*, 230(2):375–393, 2011.

[13] Yannick Gorsse, Angelo Iollo, Thomas Milcent, and Haysam Telib. A simple cartesian scheme for compressible multimaterials. *Journal of Computational Physics*, 272:772–798, 2014.

[14] G.S Jiang and C.W Shu. Efficient implementation of weighted eno schemes. *Journal of Computational Physics*, 1996.

[15] Ken Kamrin, Chris H Rycroft, and Jean-Christophe Nave. Reference map technique for finite-strain elasticity and fluid–solid interaction. *Journal of the Mechanics and Physics of Solids*, 60(11):1952–1969, 2012.

[16] Haruhiko Kohno and Jean-Christophe Nave. A new method for the level set equation using a hierarchical-gradient truncation and remapping technique. *Computer Physics Communications*, 184(6):1547–1554, 2013.

[17] Long Lee and Randall J LeVeque. An immersed interface method for incompressible navier–stokes equations. *SIAM Journal on Scientific Computing*, 25(3):832–856, 2003.

[18] John S Lowengrub, Andreas Rätz, and Axel Voigt. Phase-field modeling of the dynamics of multicomponent vesicles: Spinodal decomposition, coarsening, budding, and fission. *Physical Review E*, 79(3):031926, 2009.

[19] Emmanuel Maitre, Thomas Milcent, Georges-Henri Cottet, Annie Raoult, and Yves Usson. Applications of level set methods in computational biophysics. *Mathematical and Computer Modelling*, 49(11):2161–2169, 2009.

[20] Olivier Mercier and Jean-Christophe Nave. The characteristic mapping method for the linear advection of arbitrary sets. *arXiv preprint arXiv:1309.2731*, 2013.

[21] Charles S Peskin. The immersed boundary method. *Acta numerica*, 11:479–517, 2002.

[22] J-P Pons, Gerardo Hermosillo, Renaud Keriven, and O Faugeras. Maintaining the point correspondence in the level set framework. *Journal of Computational Physics*, 220(1):339–354, 2006.

[23] Th Richter and Th Wick. Finite elements for fluid–structure interaction in ale and fully eulerian coordinates. *Computer Methods in Applied Mechanics and Engineering*, 199(41):2633–2642, 2010.

[24] Thomas Richter. A fully eulerian formulation for fluid–structure-interaction problems. *Journal of Computational Physics*, 233:227–240, 2013.

[25] R Skalak, A Tozeren, RP Zarda, and S Chien. Strain energy function of red blood cell membranes. *Biophysical Journal*, 13(3):245–264, 1973.

[26] Boris Valkov, Chris H Rycroft, and Ken Kamrin. Eulerian method for fluid-structure interaction and submerged solid-solid contact problems. *arXiv preprint arXiv:1409.6183*, 2014.

[27] J Walter, A-V Salsac, and D Barthes-Biesel. Ellipsoidal capsules in simple shear flow: prolate versus oblate initial shapes. *Journal of Fluid Mechanics*, 676:318–347, 2011.

[28] J Walter, A-V Salsac, D Barthès-Biesel, and P Le Tallec. Coupling of finite element and boundary integral methods for a capsule in a stokes flow. *International journal for numerical methods in engineering*, 83(7):829–850, 2010.

[29] Jian-Jun Xu, Zhilin Li, John Lowengrub, and Hongkai Zhao. A level-set method for interfacial flows with surfactant. *Journal of Computational Physics*, 212(2):590–616, 2006.

[30] Yang Zhang, Ken Kamrin, and Jean-Christophe Nave. An eulerian numerical method for fluid-solid interaction. In *APS Division of Fluid Dynamics Meeting Abstracts*, volume 1, 2009.